Semarak International Journal of Nanotechnology

Journal homepage: https://semarakilmu.my/index.php/sijn/index
ISSN: 3030-6604

Exploring Pressure Dynamics in Rough-Surfaced U-Bend Pipelines: A Comparative Study of Water and Nanofluid Composites Across Varying Mass Flow Rates

Yuki Trisnoaji[1], Singgih Dwi Prasetyo[1,*], Catur Harsito[2], Abram Anggit[3], Mochamad Subchan Mauludin[4]

[1] Power Plant Engineering Technology, Faculty of Vocational Studies, State University of Malang, Malang 65145, Indonesia
[2] Department of Mechanical Computer Industrial and Management Engineering, Kangwoon National University, Republic of Korea
[3] Department of Mechanical Systems and Engineering, Gifu University, Gifu 501-1193, Japan
[4] Department of Informatics Engineering, Faculty of Engineering, Universitas Wahid Hasyim, Semarang 50236, Indonesia

ARTICLE INFO

Article history:
Received 18 November 2024
Received in revised form 28 November 2024
Accepted 26 December 2024
Available online 30 December 2024

Keywords:
Fluid dynamics; U-bend pipes; rough walls; computational fluid dynamics; ansys fluent; pressure characteristics; nanofluids; water/Al_2O_3 mixture; water/ZnO mixture; mass flow rate

ABSTRACT

This study investigates fluid flow in U-bend pipes with rough walls, an essential aspect of fluid engineering to improve system efficiency in applications such as heat exchangers and industrial piping. It compares numerical calculation results with Computational Fluid Dynamics (CFD) simulations performed in Ansys Fluent for three types of fluids: water, nano-Al_2O_3 (Water/Al_2O_3), and nano-ZnO (Water/ZnO), at mass flow rates of 0.74 kg/s, 0.75 kg/s, and 0.76 kg/s. These findings are validated against a reference value of 0.735 kg/s from Ansys. The results indicate an increase in total pressure with rising mass flow rates: water achieved the highest total pressure, ranging from 2132.72 Pa (at 0.74 kg/s) to 2252.316 Pa (at 0.76 kg/s), followed by Water/Al_2O_3, with pressures from 2100.92 Pa to 2220.59 Pa, and Water/ZnO, which had the lowest pressures ranging from 2091.69 Pa to 2208.73 Pa. ANOVA analysis reveals a significant impact of both fluid type and mass flow rate on total pressure, along with a significant interaction between the two factors. This underscores the importance of selecting appropriate combinations of fluid type and flow rate for optimal efficiency and reliability in industrial system design.

1. Introduction

Analyzing fluid flow through pipes with U-bend sections and rough walls is a crucial aspect of fluid engineering, especially regarding total pressure calculations. U-bends in pipes with rough surfaces often lead to significant pressure changes due to the formation of turbulence, flow separation, and

* *Corresponding author.*
E-mail address: singgih.prasetyo.fv@um.ac.id

https://doi.org/10.37934/sijn.3.1.121b

interactions between the fluid and surface roughness; this statement was taken from previous research [1]. This is essential for system efficiency and flow performance in heat exchangers and industrial piping systems taken in the last study [2-4].

This study comprehensively compares total pressure results from numerical calculations with those from Computational Fluid Dynamics (CFD) simulations using Ansys Fluent software. CFD allows for detailed insights into total pressure distribution in rough-walled U-bend pipes under complex flow conditions. Three types of fluids are used in this study: Water-liquid, nano-Al2O3 (Water/ Al_2O_3), and nano-ZnO (Water/ZnO). The inlet mass flow rates tested are simulated with the three fluids. The simulation results are validated against a reference mass flow rate value from Ansys to ensure the accuracy and precision of the CFD results [5,6]. The simulation results will be validated against a reference mass flow rate value from Ansys of 0.735 kg/s to ensure the accuracy and precision of the CFD results. These methods were inspired by previous study [3,7–9].

Numerical calculations and CFD simulations, such as those performed in Ansys Fluent, are vital in addressing these challenges. They allow in-depth analysis of total pressure distribution and fluid behavior under varied conditions without costly and time-intensive physical testing taken in the previous study [6]. Specifically, the integration of CFD in evaluating flow performance within U-bend pipes provides engineers with predictive insights into total pressure losses, enabling the optimization of design parameters to achieve efficient flow, reduce energy consumption, and ensure system reliability. Numerical methods, facilitated by tools like MATLAB, complement CFD by providing a quantitative foundation to validate and benchmark simulation results; a previous study inspires these methods [1,7,10,11].

To validate the simulation results from Ansys Fluent, comparisons are made with numerical calculations facilitated by MATLAB, like methods used in recent research on frictional loss and flow dynamics in pipe bends. The study is taken from the previous study [1,12–15]. Previous studies have demonstrated that validated CFD simulations offer reliable predictions of pressure distribution. However, geometric complexities and model assumptions can lead to discrepancies between the simulation and the previous study's empirical data [16]. Thus, this research aims to assess the accuracy and consistency of CFD simulations in predicting total pressure in U-bend pipes with rough walls, identifying any factors contributing to discrepancies for improved real-world model applications taken from the previous study [17–19]. Despite numerous studies on fluid flow and pressure distribution in pipe bends, there is still a significant gap in understanding the combined effects of surface roughness and U-bend geometry on total pressure calculations. This study addresses this gap by providing a detailed comparison between numerical calculations and CFD simulations, offering insights into the complexities of flow behavior in such configurations. The findings of this study, which highlight the importance of selecting appropriate fluid and flow rate combinations for optimal efficiency and reliability in industrial applications, have significant practical implications for fluid engineering.

2. Set the Stage for Current Research

The study of fluid flow within U-bend pipes with rough walls is critical in fluid engineering due to the significant impact of surface roughness on turbulence, flow separation, and pressure loss; this case is taken from the previous study and modified [4,20,21]. This configuration often leads to complex flow phenomena that influence overall system efficiency, making it essential to accurately assess total pressure distribution in such settings. Applications such as heat exchangers and industrial piping systems are particularly affected, as pressure variations can substantially impact system performance in the previous study [22].

Computational fluid dynamics (CFD) techniques have become invaluable for detailed analysis of the impact of pipe geometry and surface properties on flow characteristics. This study leverages these advanced tools to provide a comprehensive understanding of fluid flow within U-bend pipes with rough walls [1]. Advanced turbulence models, such as Reynolds-Averaged Navier-Stokes (RANS) and Large Eddy Simulation (LES), have been widely used to improve the accuracy of predictions for turbulent flow and pressure behavior in U-bend pipes taken in the previous study [21,23]. Previous studies show that validated CFD simulations yield reliable predictions of total pressure distributions, although specific challenges arise due to geometric complexities and the assumptions inherent in modeling techniques. This study is taken from a previous study [8]. This research aims to evaluate the reliability of CFD simulation methods in predicting total pressure in U-bend pipes with rough walls and to enhance models for more accurate real-world applications inspired by the previous study [1,24].

3. Methodology

3.1 Flowchart and Specific Geometry

Figure 1 (a) illustrates the research methodology flowchart, detailing each step from model development to simulation and validation. Figure 1 (b) shows the U-bend geometry used in the study, specifying the dimensions and characteristics essential for analyzing fluid flow behavior [16].

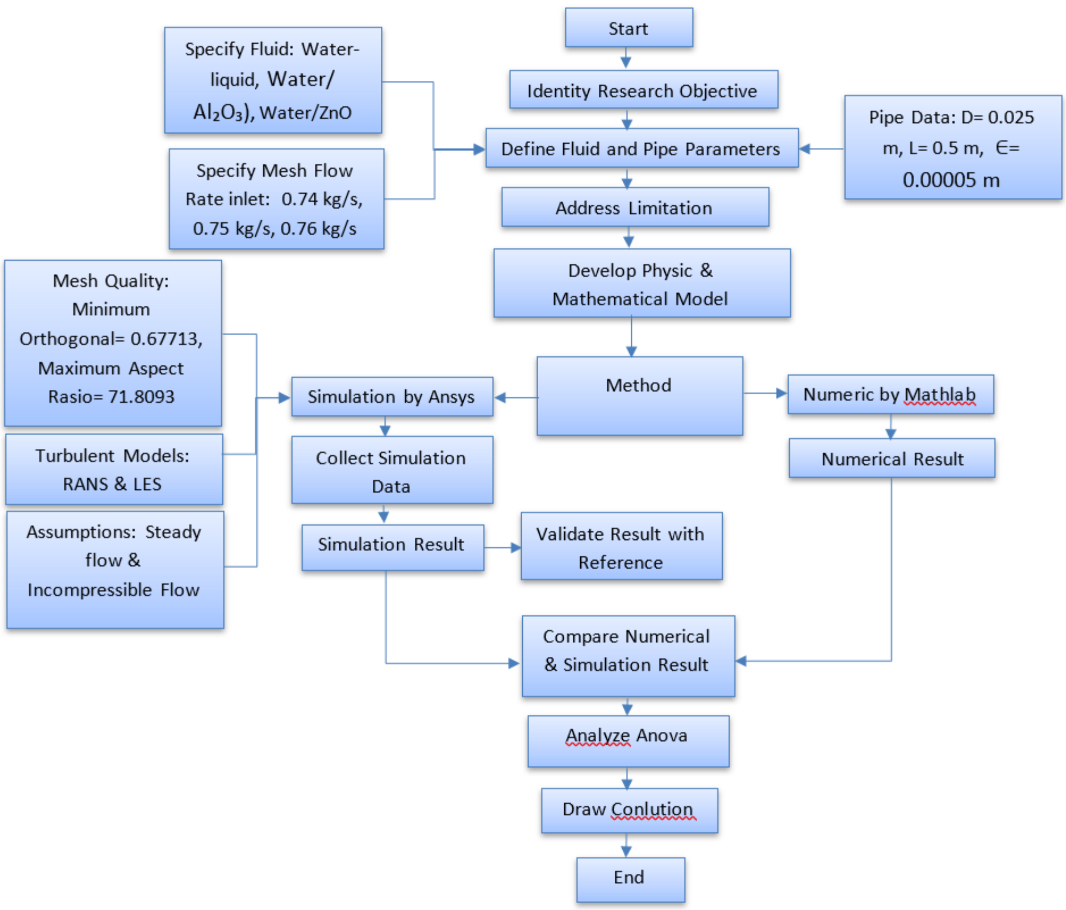

(a)

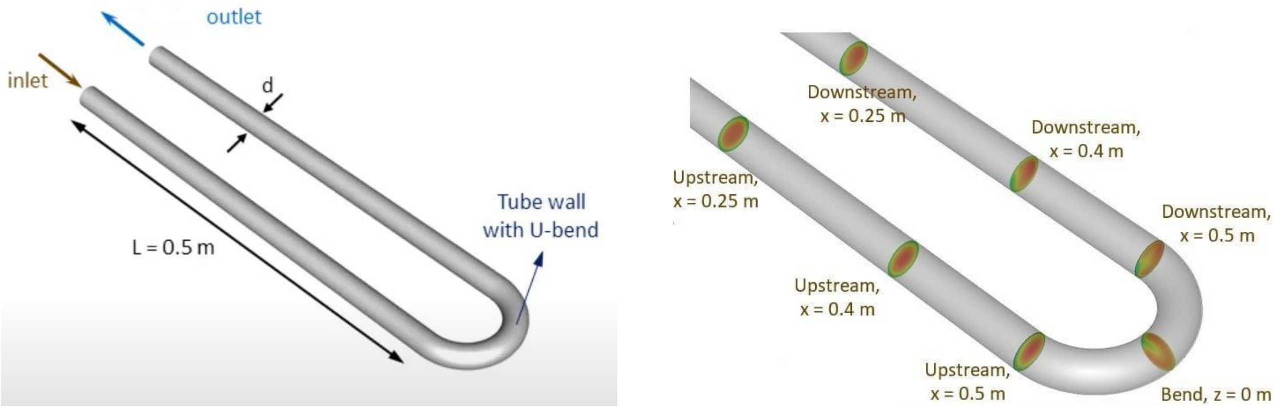

(b)

Fig. 1. (a) The flowchart method (b) Specific geometry

3.1.1 Flowchart explanation

This flowchart illustrates a systematic research process for analyzing pipe fluid flow using numerical methods and CFD simulations. The study begins by identifying research objectives and developing mathematical models to explain the physical phenomena under investigation. In the Define Fluid and Pipe Parameters stage, fluid properties and pipe parameters are specified, including the type of fluid (water, nano-Al_2O_3, and nano-ZnO), variations in mass flow rate (0.74 kg/s, 0.75 kg/s, and 0.76 kg/s), and pipe details (diameter 0.025 m, length 0.5 m, and roughness 0.00005 m). At this stage, an Address Limitations step is added to acknowledge potential limitations in the study, such as the impact of surface roughness variations and assumptions in the CFD model. This transparency strengthens the research quality by clarifying the analysis's limitations.

After defining these parameters, a numerical method is applied using MATLAB to solve the initial mathematical model, and results are stored for comparison. Further CFD simulations are conducted in ANSYS using turbulence models such as RANS and LES for enhanced accuracy. At the same time, mesh quality is ensured with a minimum orthogonal quality of 0.627713 and a maximum aspect ratio of 71.8093. Steady-state and incompressible flow assumptions are also applied in this simulation. The simulation data is then collected, validated against reference data, and compared with the numerical results to assess discrepancies. The study concludes with an analysis of the effect of inlet mass flow rate on outcomes, followed by conclusions that summarize the critical findings of the research.

3.2 Address Limitation

The author needs to acknowledge the limitations of this study. With this transparency, the overall quality of the research can be strengthened. Here are some limitations that need to be acknowledged:

i. Surface Roughness Variability: This study assumes uniform surface roughness on the U-bend pipe. However, variations in surface roughness in real-world applications can affect flow dynamics and pressure distribution, which may lead to simulation results differing from actual conditions.
ii. Assumptions in the CFD Model: The CFD model is based on several assumptions to simplify the complexity of fluid flow, including ideal boundary conditions, steady flow,

and the neglect of some minor forces. These assumptions may not capture all aspects of real-world fluid behavior and can introduce errors or oversimplifications.

iii. Mesh Quality and Grid Independence: The accuracy of simulation results heavily depends on mesh quality and grid independence. The results may need to be improved to achieve a fine mesh or ensure grid independence.

iv. Nanoparticle Distribution: This study assumes a uniform distribution of nanoparticles in the fluid, whereas, in reality, nanoparticles may cluster or become unevenly distributed due to various factors, potentially affecting the fluid's viscosity, thermal conductivity, and pressure distribution.

v. Validation Against Experimental Data: Validation of simulation results against numerical calculations rather than direct experimental data may overlook discrepancies that could arise in physical experiments due to unexpected factors or real-world complexities.

Acknowledging these limitations provides a deeper understanding of the study's findings and suggests areas for further research to address these potential gaps. This transparency not only strengthens the credibility of the research but also aids future studies in building upon and improving the existing work.

3.3 Table Properties of Fluid

Table 1 presents data on the physical properties of various fluids, including water and air mixtures with Al2O3 and ZnO nanoparticles taken from the book at [25].

Table 1
Properties of Fluid

Fluid	Density(ρ)	Specific Heat (Cp) J/kg k	Thermal Conductivity W/m k	Viscosity (μ) Ns/m^2
Water-Liquid	998.2	4182	0.6	0.001003
Water/Al_2O_3	1006	4145.3	0.613	0.001002
Water/ZnO	1010	4120	0.619	0.00103

3.4 The Physics Formula

The following is the formula for numerical calculations taken from the book at [25].

Find A: $A = \pi \times \left(\frac{D}{2}\right)^2$ (1)

Find v : $v = \frac{\dot{m}}{\rho \times A}$ (2)

Find Re Number: $Re = \frac{(\rho \times v \times D)}{\mu}$ (3)

Find f: $\frac{1}{\sqrt{f}} = -2\log_{10}(\frac{\epsilon}{D}/3.7\frac{2.51}{Re\sqrt{f}}$ (4)

The numerical solution of the Colebrook equation is often obtained using iterative or numerical methods. The specific MATLAB function used here is vpasolve, which finds numerical solutions to equations; this solution formula is taken from a previous study [10,25–27]. In a more concise numerical form, the implementation using MATLAB can be represented as follows:

Define the Colebrook Function:

$$Colebrook(f) = \frac{1}{\sqrt{f}} + 2\log_{10}(\frac{\in/D}{3.7}\frac{2.51}{Re\sqrt{f}}) = 0 \quad (5)$$

Solve for f:

$$(f) = vpasolve\ (colebrook\ (f), f, [0, 1] \quad (6)$$

Final Numerical Formulation:

$$(f) = double\ (vpasolve\ (\frac{1}{\sqrt{f}} + 2\log_{10}(\frac{\in/D}{3.7}\frac{2.51}{Re\sqrt{f}}) = 0, f, [0, 1] \quad (7)$$

In the context of MATLAB, double(vpasolve(...)) is used to find a numerical solution to an equation and then convert that solution into a double data type (a floating-point number); this solution formula is taken from a previous study [10].

Find ΔP:

$$\Delta P = f\ \times \left(\frac{L}{D}\right) \times (\rho\ \times \frac{v^2}{2}) \quad (8)$$

4. Results

4.1 Calculation by Matlab

The numerical calculations in this study will be assisted by MATLAB, a powerful computational tool for efficiently performing complex mathematical analyses. MATLAB will facilitate the resolution of equations, including the Colebrook equation, allowing for accurate and reliable numerical solutions [26,27]. This software's capabilities will enhance fluid dynamics analysis, enabling the assessment of parameters such as friction factors and flow rates in various fluid scenarios. By leveraging MATLAB, we aim to ensure precision in our calculations and streamline the overall research process.

The first fluid, water-liquid, shows in Figure 2 an increase in total pressure with the rise in inlet mass flow rate. At a mass flow rate inlet of 0.74 kg/s, the total pressure reaches 1130.59 Pa, while an increase to 0.75 kg/s results in a total pressure of 1161.04 Pa. Additionally, there is a data point at the same mass flow rate of 0.76 kg/s, yielding a higher total pressure of 1191.9 Pa. This increase aligns with the theory that higher mass flow rates raise pressure due to added kinetic energy and fluid-wall friction along the pipe; the theory is taken from the previous study [13].

The second fluid, the Water/Al_2O_3 mixture, also shows a Figure 3 increase in total pressure as the inlet mass flow rate rises. At 0.74 kg/s, the total pressure is 1121.8 Pa, increasing to 1152.014 Pa at 0.75 kg/s and reaching 1182.63 Pa at a mass flow rate of 0.76 kg/s. Although the pressure increase trend with mass flow rate is similar to water-liquid, the Water/Al_2O_3 fluid generally shows slightly lower pressures at the same flow rate. This can be attributed to the presence of Water/Al_2O_3 particles, which may increase energy dissipation within the flow and raise the fluid's effective viscosity, thus requiring less pressure to maintain flow compared to pure water; this theory is taken from the previous study [2].

Figure 4 is the third fluid, the Water/ZnO mixture, which exhibits an upward trend in pressure with an increased inlet mass flow rate, though the values are generally lower than those of the other two fluids. At a mass flow rate of 0.74 kg/s, the pressure is 1117.38 Pa, increasing to 1147.474 Pa at 0.75 kg/s. An additional data point at 0.76 kg/s shows a higher total pressure of 1177.97 Pa. This trend reflects a similar pattern to the other fluids, though with lower pressure values, possibly due to Water/ZnO particles in the mixture influencing flow characteristics; this theory is taken from the previous study [9].

```
>> % Input parameters
rho = 998.2; % kg/m^3
mu = 0.001003; % Pa·s
D = 0.025; % m
L = 0.5; % m
epsilon = 0.0005; % m
mass_flow_rate = 0.74; % kg/s

% Calculate cross-sectional area
A = pi * (D / 2)^2;

% Calculate velocity
v = mass_flow_rate / (rho * A);

% Calculate Reynolds number
Re = (rho * v * D) / mu;
```

```
% Calculate friction factor using Colebrook-White equation
syms f
colebrook = @(f) 1/sqrt(f) + 2*log10((epsilon/D)/3.7 + 2.51/(Re*sqrt(f)));
f = double(vpasolve(colebrook(f), f, [0 1]));

% Calculate pressure loss using Darcy-Weisbach equation
delta_P = f * (L/D) * (rho * v^2 / 2);

% Display results
fprintf('Cross-sectional Area (A): %f m²\n', A);
fprintf('Velocity (v): %f m/s\n', v);
fprintf('Reynolds Number (Re): %f\n', Re);
fprintf('Friction Factor (f): %f\n', f);
fprintf('Pressure Loss (ΔP): %f Pa\n', delta_P);
Cross-sectional Area (A): 0.000491 m²
Velocity (v): 1.510234 m/s
Reynolds Number (Re): 37575.165029
Friction Factor (f): 0.049659
Pressure Loss (ΔP): 1130.587595 Pa
fx >>
```

(a)

```
>> % Input parameters
rho = 998.2; % kg/m^3
mu = 0.001003; % Pa·s
D = 0.025; % m
L = 0.5; % m
epsilon = 0.0005; % m
mass_flow_rate = 0.75; % kg/s

% Calculate cross-sectional area
A = pi * (D / 2)^2;

% Calculate velocity
v = mass_flow_rate / (rho * A);

% Calculate Reynolds number
Re = (rho * v * D) / mu;
```

```
% Calculate friction factor using Colebrook-White equation
syms f
colebrook = @(f) 1/sqrt(f) + 2*log10((epsilon/D)/3.7 + 2.51/(Re*sqrt(f)));
f = double(vpasolve(colebrook(f), f, [0 1]));

% Calculate pressure loss using Darcy-Weisbach equation
delta_P = f * (L/D) * (rho * v^2 / 2);

% Display results
fprintf('Cross-sectional Area (A): %f m²\n', A);
fprintf('Velocity (v): %f m/s\n', v);
fprintf('Reynolds Number (Re): %f\n', Re);
fprintf('Friction Factor (f): %f\n', f);
fprintf('Pressure Loss (ΔP): %f Pa\n', delta_P);
Cross-sectional Area (A): 0.000491 m²
Velocity (v): 1.530643 m/s
Reynolds Number (Re): 38082.937529
Friction Factor (f): 0.049646
Pressure Loss (ΔP): 1161.038606 Pa
fx >>
```

(b)

```
>> % Input parameters
rho = 998.2; % kg/m^3
mu = 0.001003; % Pa·s
D = 0.025; % m
L = 0.5; % m
epsilon = 0.0005; % m
mass_flow_rate = 0.76; % kg/s

% Calculate cross-sectional area
A = pi * (D / 2)^2;

% Calculate velocity
v = mass_flow_rate / (rho * A);

% Calculate Reynolds number
Re = (rho * v * D) / mu;
```

```
% Calculate friction factor using Colebrook-White equation
syms f
colebrook = @(f) 1/sqrt(f) + 2*log10((epsilon/D)/3.7 + 2.51/(Re*sqrt(f)));
f = double(vpasolve(colebrook(f), f, [0 1]));

% Calculate pressure loss using Darcy-Weisbach equation
delta_P = f * (L/D) * (rho * v^2 / 2);

% Display results
fprintf('Cross-sectional Area (A): %f m²\n', A);
fprintf('Velocity (v): %f m/s\n', v);
fprintf('Reynolds Number (Re): %f\n', Re);
fprintf('Friction Factor (f): %f\n', f);
fprintf('Pressure Loss (ΔP): %f Pa\n', delta_P);
Cross-sectional Area (A): 0.000491 m²
Velocity (v): 1.551051 m/s
Reynolds Number (Re): 38590.710030
Friction Factor (f): 0.049633
Pressure Loss (ΔP): 1191.894056 Pa
>>
```

(c)

Fig. 2. The result numeric calculation of water-liquid for (a) 0.74 kg/s, (b) 0.75 kg/s, (c) 0.76 kg/s

```
>> % Input parameters
rho = 1006; % kg/m^3
mu = 0.001002; % Pa·s
D = 0.025; % m
L = 0.5; % m
epsilon = 0.0005; % m
mass_flow_rate = 0.74; % kg/s

% Calculate cross-sectional area
A = pi * (D / 2)^2;

% Calculate velocity
v = mass_flow_rate / (rho * A);

% Calculate Reynolds number
Re = (rho * v * D) / mu;
```

```
% Calculate friction factor using Colebrook-White equation
syms f
colebrook = @(f) 1/sqrt(f) + 2*log10((epsilon/D)/3.7 + 2.51/(Re*sqrt(f)));
f = double(vpasolve(colebrook(f), f, [0 1]));

% Calculate pressure loss using Darcy-Weisbach equation
delta_P = f * (L/D) * (rho * v^2 / 2);

% Display results
fprintf('Cross-sectional Area (A): %f m²\n', A);
fprintf('Velocity (v): %f m/s\n', v);
fprintf('Reynolds Number (Re): %f\n', Re);
fprintf('Friction Factor (f): %f\n', f);
fprintf('Pressure Loss (ΔP): %f Pa\n', delta_P);
Cross-sectional Area (A): 0.000491 m²
Velocity (v): 1.498524 m/s
Reynolds Number (Re): 37612.665194
Friction Factor (f): 0.049658
Pressure Loss (ΔP): 1121.799087 Pa
```

(a)

```
>> % Input parameters
rho = 1006; % kg/m^3
mu = 0.001002; % Pa·s
D = 0.025; % m
L = 0.5; % m
epsilon = 0.0005; % m
mass_flow_rate = 0.75; % kg/s

% Calculate cross-sectional area
A = pi * (D / 2)^2;

% Calculate velocity
v = mass_flow_rate / (rho * A);

% Calculate Reynolds number
Re = (rho * v * D) / mu;
```

```
% Calculate friction factor using Colebrook-White equation
syms f
colebrook = @(f) 1/sqrt(f) + 2*log10((epsilon/D)/3.7 + 2.51/(Re*sqrt(f)));
f = double(vpasolve(colebrook(f), f, [0 1]));

% Calculate pressure loss using Darcy-Weisbach equation
delta_P = f * (L/D) * (rho * v^2 / 2);

% Display results
fprintf('Cross-sectional Area (A): %f m²\n', A);
fprintf('Velocity (v): %f m/s\n', v);
fprintf('Reynolds Number (Re): %f\n', Re);
fprintf('Friction Factor (f): %f\n', f);
fprintf('Pressure Loss (ΔP): %f Pa\n', delta_P);
Cross-sectional Area (A): 0.000491 m²
Velocity (v): 1.518775 m/s
Reynolds Number (Re): 38120.944453
Friction Factor (f): 0.049645
Pressure Loss (ΔP): 1152.013680 Pa
```

(b)

```
>> % Input parameters
rho = 1006; % kg/m^3
mu = 0.001002; % Pa·s
D = 0.025; % m
L = 0.5; % m
epsilon = 0.0005; % m
mass_flow_rate = 0.76; % kg/s

% Calculate cross-sectional area
A = pi * (D / 2)^2;

% Calculate velocity
v = mass_flow_rate / (rho * A);

% Calculate Reynolds number
Re = (rho * v * D) / mu;
```

```
% Calculate friction factor using Colebrook-White equation
syms f
colebrook = @(f) 1/sqrt(f) + 2*log10((epsilon/D)/3.7 + 2.51/(Re*sqrt(f)));
f = double(vpasolve(colebrook(f), f, [0 1]));

% Calculate pressure loss using Darcy-Weisbach equation
delta_P = f * (L/D) * (rho * v^2 / 2);

% Display results
fprintf('Cross-sectional Area (A): %f m²\n', A);
fprintf('Velocity (v): %f m/s\n', v);
fprintf('Reynolds Number (Re): %f\n', Re);
fprintf('Friction Factor (f): %f\n', f);
fprintf('Pressure Loss (ΔP): %f Pa\n', delta_P);
Cross-sectional Area (A): 0.000491 m²
Velocity (v): 1.539025 m/s
Reynolds Number (Re): 38629.223713
Friction Factor (f): 0.049632
Pressure Loss (ΔP): 1182.629576 Pa
```

(c)

Fig. 3. The result numeric calculation of water/ Al_2O_3 for (a) 0.74 kg/s, (b) 0.75 kg/s, (c) 0.76 kg/s

```
>> % Input parameters
rho = 1010; % kg/m^3
mu = 0.001003; % Pa·s
D = 0.025; % m
L = 0.5; % m
epsilon = 0.0005; % m
mass_flow_rate = 0.74; % kg/s

% Calculate cross-sectional area
A = pi * (D / 2)^2;

% Calculate velocity
v = mass_flow_rate / (rho * A);

% Calculate Reynolds number
Re = (rho * v * D) / mu;
```

```
% Calculate friction factor using Colebrook-White equation
syms f
colebrook = @(f) 1/sqrt(f) + 2*log10((epsilon/D)/3.7 + 2.51/(Re*sqrt(f)));
f = double(vpasolve(colebrook(f), f, [0 1]));

% Calculate pressure loss using Darcy-Weisbach equation
delta_P = f * (L/D) * (rho * v^2 / 2);

% Display results
fprintf('Cross-sectional Area (A): %f m²\n', A);
fprintf('Velocity (v): %f m/s\n', v);
fprintf('Reynolds Number (Re): %f\n', Re);
fprintf('Friction Factor (f): %f\n', f);
fprintf('Pressure Loss (ΔP): %f Pa\n', delta_P);
Cross-sectional Area (A): 0.000491 m²
Velocity (v): 1.492590 m/s
Reynolds Number (Re): 37575.165029
Friction Factor (f): 0.049659
Pressure Loss (ΔP): 1117.378750 Pa
```

(a)

```
>> % Input parameters
rho = 1010; % kg/m^3
mu = 0.001003; % Pa·s
D = 0.025; % m
L = 0.5; % m
epsilon = 0.0005; % m
mass_flow_rate = 0.75; % kg/s

% Calculate cross-sectional area
A = pi * (D / 2)^2;

% Calculate velocity
v = mass_flow_rate / (rho * A);

% Calculate Reynolds number
Re = (rho * v * D) / mu;
```

```
% Calculate friction factor using Colebrook-White equation
syms f
colebrook = @(f) 1/sqrt(f) + 2*log10((epsilon/D)/3.7 + 2.51/(Re*sqrt(f)));
f = double(vpasolve(colebrook(f), f, [0 1]));

% Calculate pressure loss using Darcy-Weisbach equation
delta_P = f * (L/D) * (rho * v^2 / 2);

% Display results
fprintf('Cross-sectional Area (A): %f m²\n', A);
fprintf('Velocity (v): %f m/s\n', v);
fprintf('Reynolds Number (Re): %f\n', Re);
fprintf('Friction Factor (f): %f\n', f);
fprintf('Pressure Loss (ΔP): %f Pa\n', delta_P);
Cross-sectional Area (A): 0.000491 m²
Velocity (v): 1.512760 m/s
Reynolds Number (Re): 38082.937529
Friction Factor (f): 0.049646
Pressure Loss (ΔP): 1147.473997 Pa
```

(b)

```
>> % Input parameters
rho = 1010; % kg/m^3
mu = 0.001003; % Pa·s
D = 0.025; % m
L = 0.5; % m
epsilon = 0.0005; % m
mass_flow_rate = 0.76; % kg/s

% Calculate cross-sectional area
A = pi * (D / 2)^2;

% Calculate velocity
v = mass_flow_rate / (rho * A);

% Calculate Reynolds number
Re = (rho * v * D) / mu;
```

```
% Calculate friction factor using Colebrook-White equation
syms f
colebrook = @(f) 1/sqrt(f) + 2*log10((epsilon/D)/3.7 + 2.51/(Re*sqrt(f)));
f = double(vpasolve(colebrook(f), f, [0 1]));

% Calculate pressure loss using Darcy-Weisbach equation
delta_P = f * (L/D) * (rho * v^2 / 2);

% Display results
fprintf('Cross-sectional Area (A): %f m²\n', A);
fprintf('Velocity (v): %f m/s\n', v);
fprintf('Reynolds Number (Re): %f\n', Re);
fprintf('Friction Factor (f): %f\n', f);
fprintf('Pressure Loss (ΔP): %f Pa\n', delta_P);
Cross-sectional Area (A): 0.000491 m²
Velocity (v): 1.532930 m/s
Reynolds Number (Re): 38590.710030
Friction Factor (f): 0.049633
Pressure Loss (ΔP): 1177.968957 Pa
```

(c)

Fig. 4. The result numeric calculation of water/ ZnO for (a) 0.74 kg/s, (b) 0.75 kg/s, (c) 0.76 kg/s

4.2 Simulation Result

The simulations in this study will be conducted using ANSYS Fluent, a powerful computational fluid dynamics software known for its ability to accurately model complex fluid flow scenarios. ANSYS Fluent will facilitate the analysis of total pressure in systems involving U-bends, allowing for a detailed investigation of pressure distribution and losses due to changes in flow direction. This software's capabilities will enhance our understanding of fluid dynamics by enabling the assessment of parameters such as friction factors and flow rates in these critical flow geometries. By leveraging ANSYS Fluent, we aim to achieve precise simulations that will inform our analysis of total pressure variations and streamline the overall research process.

Figure 5 consists of a contour plot and a table illustrating the total pressure distribution in a water-liquid flow simulation using Ansys, with a mass flow rate of 0.735 kg/s. The contour plot shows a U-shaped pipe where the pressure decreases from 4288.46 Pa at the inlet to 214.03 Pa along its length, indicating energy loss due to friction and flow resistance. The table lists area-weighted average total pressure values at various locations, highlighting the highest pressure at the inlet (4259.1769 Pa) and the lowest at the outlet (1169.3139 Pa).

The first fluid in Figure 6, water-liquid, consistently increases total pressure as the inlet mass flow rate rises. At a mass flow rate of 0.74 kg/s, the total pressure is 2132.72 Pa; increasing the flow rate to 0.75 kg/s raises the total pressure to 2192.324 Pa, and a further rise to 0.76 kg/s yields a total pressure of 2252.316 Pa. This steady increase aligns with theoretical expectations, as a higher mass flow rate generally raises kinetic energy and the fluid's interaction with rough walls, leading to higher total pressures. Water-liquid's relatively high-pressure values can be attributed to the fluid's density and increased wall friction, especially in curved sections, which amplify pressure demands along the pipe's flow path; this theory is taken from the previous study [28,29].

Figure 7 is the second fluid, a mixture of Water/Al_2O_3, which also shows an increase in total pressure with rising mass flow rates, although the values are slightly lower than those of water-liquid at each corresponding flow rate. For Water/Al_2O_3, a mass flow rate of 0.74 kg/s produces a total pressure of 2100.92 Pa, which rises to 2158.96 Pa at 0.75 kg/s, and further to 2220.59 Pa at 0.76 kg/s. The lower pressure compared to pure water can be linked to the presence of Water/Al_2O_3/nanoparticles, which increase the fluid's effective viscosity and thermal conductivity, affecting energy dissipation. The Water/Al_2O_3 particles help slightly reduce the total pressure required to maintain flow, as their presence enhances internal fluid dynamics and modifies the interaction with pipe walls; this theory is taken from the previous study [28].

Figure 8 is the third fluid, the Water/ZnO mixture, which shows a similar trend, with total pressure increasing as the mass flow rate rises, though the pressure values are the lowest among the three fluids. At a mass flow rate of 0.74 kg/s, the total pressure is 2091.69 Pa, increasing to 2149.15 Pa at 0.75 kg/s and reaching 2208.73 Pa at 0.76 kg/s. The lower pressure readings compared to Water-liquid and Water/Al_2O_3 suggest that Water/ZnO particles produce slightly less resistance in the flow, leading to reduced total pressure. This characteristic may make Water/ZnO mixtures advantageous in systems requiring lower pressure loads, as water/ZnO particles in the fluid provide stable flow characteristics while generating less wall pressure, possibly enhancing efficiency in applications with curved piping; this theory is taken from the previous study [30].

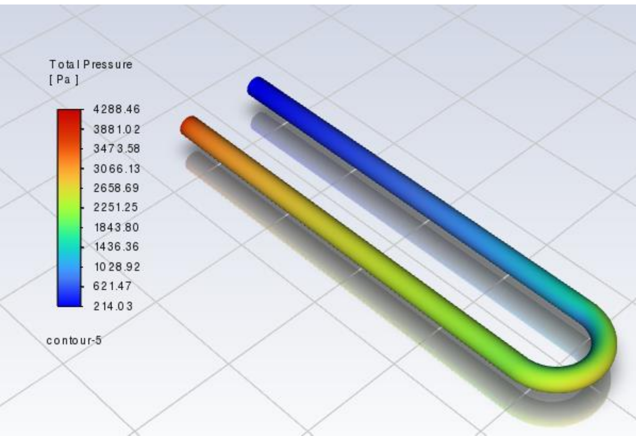

Area-Weighted Average Total Pressure	[Pa]
downstream-plane	2442.8495
inlet	4259.1769
outlet	1169.313
upstream-plane	3077.6419
walls-bend	2055.5231
walls-straight	1746.9499
x=0.25	2687.4984
x=0.4	2707.1267
y=0	2874.0322
z=0	2826.4641
Net	2075.2227

(a) (b)

Fig. 5. The result of reference by Ansys the fluid is water-liquid (a) Contour 0.735 kg/s, and (b) Total Pressure 0.735 kg/s

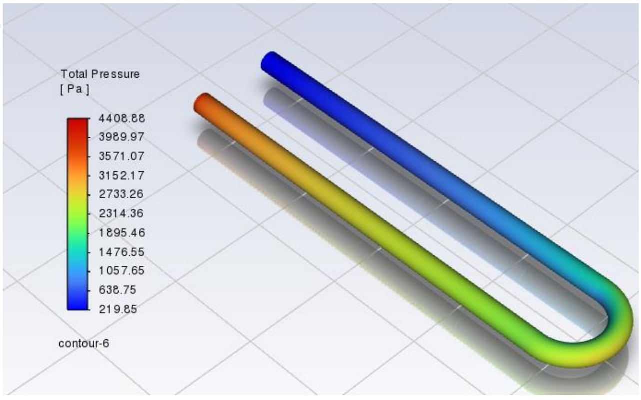

Area-Weighted Average Total Pressure	[Pa]
downstream-plane	2510.0092
inlet	4377.9115
outlet	1200.6843
upstream-plane	3162.1898
walls-bend	2112.6597
walls-straight	1795.6539
x=0.25	2761.4154
x=0.4	2781.5964
y=0	2953.0228
z=0	2904.043
Net	2132.7628

(a)

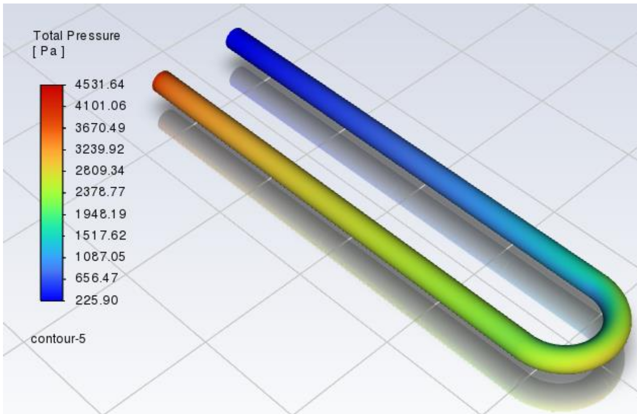

Area-Weighted Average Total Pressure	[Pa]
downstream-plane	2579.6485
inlet	4499.8268
outlet	1233.3614
upstream-plane	3249.8327
walls-bend	2171.8205
walls-straight	1846.0121
x=0.25	2838.0615
x=0.4	2858.8038
y=0	3034.9316
z=0	2984.4796
Net	2192.3238

(b)

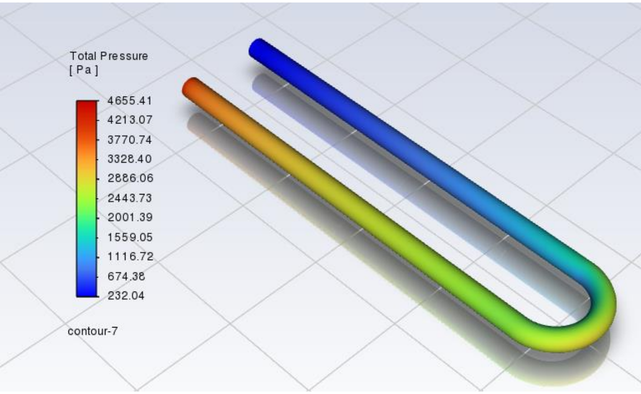

Area-Weighted Average Total Pressure	[Pa]
downstream-plane	2649.8783
inlet	4622.7402
outlet	1266.4834
upstream-plane	3338.1932
walls-bend	2231.3875
walls-straight	1896.6773
x=0.25	2915.3592
x=0.4	2936.6547
y=0	3117.5676
z=0	3065.5909
Net	2252.3126

(c)

Fig. 6. The result contour and total pressure of simulation of the fluid is water-liquid with the mass flow rate inlet for (a) 0.74 kg/s, (b) 0.75 kg/s, (c) 0.76 kg/s

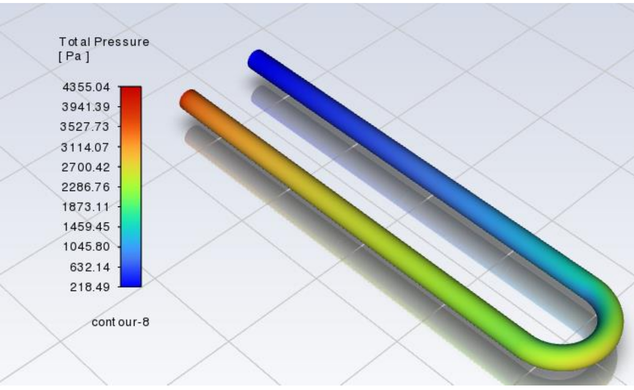

Calculation complete.

Area-Weighted Average Total Pressure	[Pa]
downstream-plane	2481.3932
inlet	4324.2757
outlet	1194.3871
upstream-plane	3122.7136
walls-bend	2081.5746
walls-straight	1766.8873
x=0.25	2724.0649
x=0.4	2745.7226
y=0	2912.9365
z=0	2867.9201
Net	2100.9229

(a)

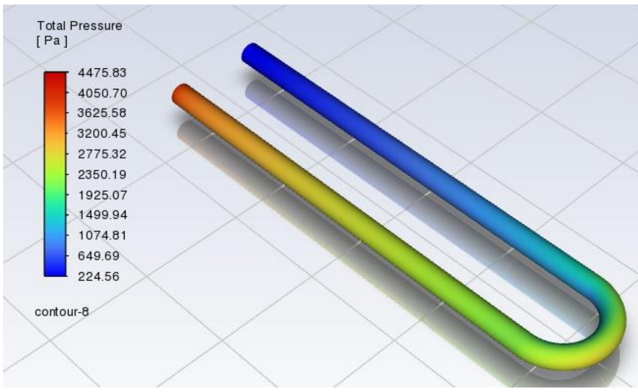

Area-Weighted Average Total Pressure	[Pa]
downstream-plane	2549.4338
inlet	4444.2202
outlet	1227.174
upstream-plane	3208.5583
walls-bend	2138.8957
walls-straight	1815.7897
x=0.25	2799.2228
x=0.4	2821.2581
y=0	2993.2627
z=0	2946.6169
Net	2158.9596

(b)

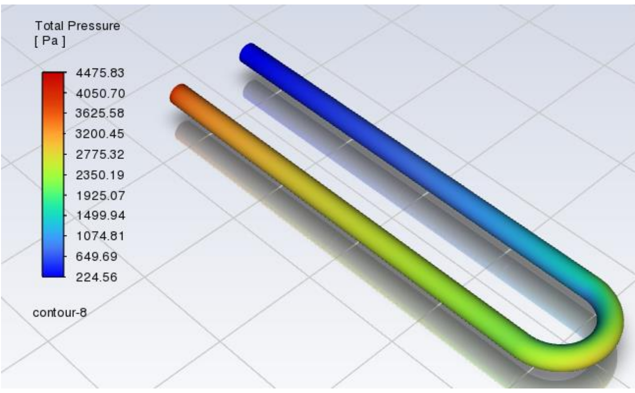

Area-Weighted Average Total Pressure	[Pa]
downstream-plane	2621.2317
inlet	4569.7344
outlet	1259.9982
upstream-plane	3298.8935
walls-bend	2200.3724
walls-straight	1868.1627
x=0.25	2877.9722
x=0.4	2900.7784
y=0	3077.26
z=0	3029.4549
Net	2220.5893

(c)

Fig. 7. The result contour and total pressure of simulation of the fluid is water- Al_2O_3 with the mass flow rate inlet for (a) 0.74 kg/s, (b) 0.75 kg/s, (c) 0.76 kg/s

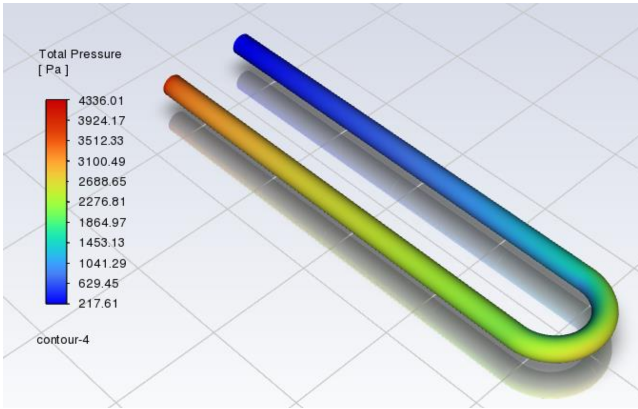

Area-Weighted Average Total Pressure	[Pa]
downstream-plane	2470.8499
inlet	4305.3793
outlet	1189.8176
upstream-plane	3109.408
walls-bend	2072.2847
walls-straight	1758.9787
x=0.25	2712.4631
x=0.4	2734.0023
y=0	2900.5456
z=0	2855.7696
Net	2091.6944

(a)

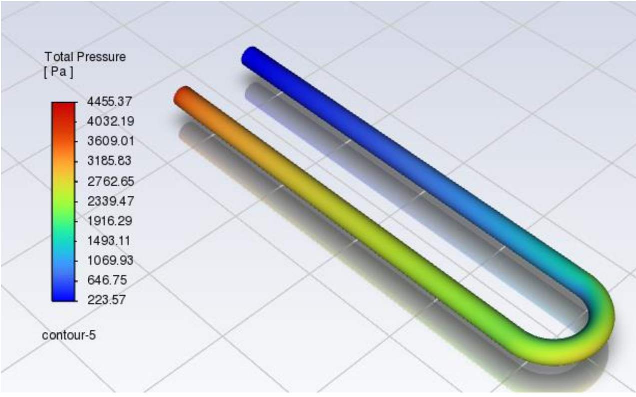


```
Calculation complete.

                Area-Weighted Average
                           Total Pressure                   [Pa]
-------------------------------- --------------------
                  downstream-plane            2538.3897
                             inlet            4423.8931
                            outlet            1222.1057
                     upstream-plane           3194.5156
                        walls-bend            2129.2969
                    walls-straight            1807.3772
                            x=0.25            2786.7443
                             x=0.4            2808.8486
                               y=0            2980.0164
                               z=0            2933.8356
                  ---------------- --------------------
                               Net            2149.1552
```

(b)

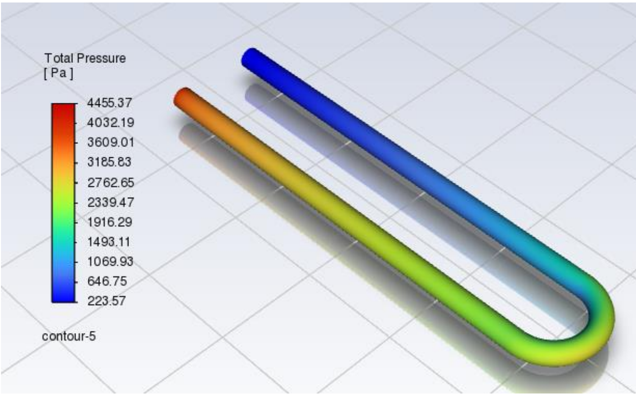


```
                Area-Weighted Average
                           Total Pressure                   [Pa]
-------------------------------- --------------------
                  downstream-plane            2608.0251
                             inlet            4546.565
                            outlet            1255.1678
                     upstream-plane           3282.305
                        walls-bend            2188.2285
                    walls-straight            1857.7193
                            x=0.25            2863.5838
                             x=0.4            2886.1243
                               y=0            3062.0773
                               z=0            3014.3196
                  ---------------- --------------------
                               Net            2208.7261
```

(c)

Fig. 8. The result contour and total pressure of simulation of the fluid is water- ZnO with the mass flow rate inlet for (a) 0.74 kg/s, (b) 0.75 kg/s, (c) 0.76 kg/s

Figure 9 illustrates the simulation validation results for three types of fluids: water-liquid, Water/ Al_2O_3, and Water/ZnO, tested at inlet mass flow rates of 0.74 kg/s, 0.75 kg/s, and 0.76 kg/s. The horizontal axis represents the variation in mass flow rate, while the vertical axis indicates the percentage error in the simulation results relative to reference values. At a lower mass flow rate (0.74 kg/s), Water-liquid exhibits an error of 2.77%, followed by Water/ Al_2O_3, 1.24%, and Water/ZnO, 0.79%. However, as the mass flow rate increases to 0.75 kg/s and 0.76 kg/s, a notable rise in error occurs for all three fluids. This increase is most pronounced in Water-liquid, reaching an error of 8.53% at 0.76 kg/s, while Water/Al_2O_3 and Water/ZnO record errors of 6.99% and 6.43%, respectively, at the same rate, this theory is taken the previous study [31].

The consistent rising error pattern across all three fluids indicates a direct relationship between mass flow rate and the degree of simulation deviation. These results suggest that the simulation for water-liquid demonstrates the highest inaccuracy compared to the other two fluids, with Water/ZnO showing more stable and accurate performance across all tested mass flow rates; this theory is taken from the previous study [15]. This finding implies that the thermophysical properties and characteristics of Water/ZnO contribute to a more stable simulation outcome compared to Water-liquid and Water/Al_2O_3; this theory is taken from the previous study [9].

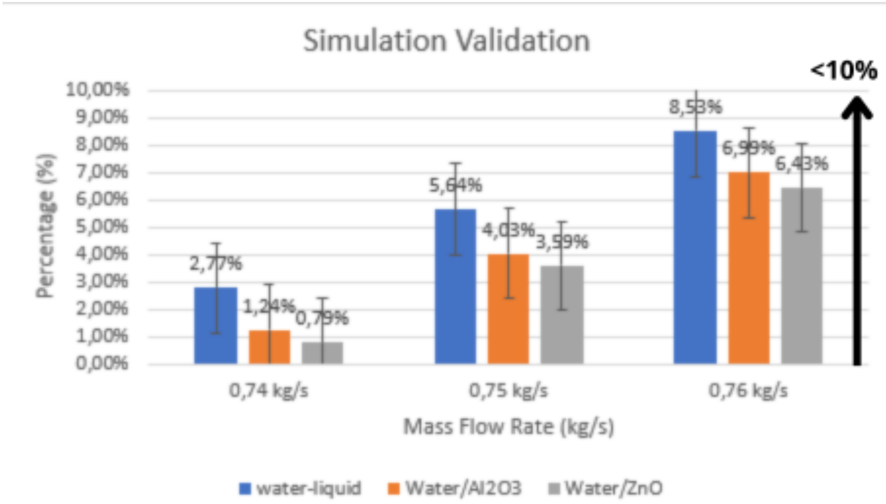

Fig. 9. Simulation validation of ANSYS reference data with simulation results

4.3 Graphic Comparison of Numerical Calculations with Simulations

Figure 10 analyzes the differences between numerical calculations and simulation results for total pressure (Pa) at various mass flow rates (0.74 kg/s, 0.75 kg/s, and 0.76 kg/s) across three different fluids: Water-liquid, Water/Al_2O_3 Fluid, and Water/ZnO Fluid. The comparison indicates that the simulation results consistently show higher total pressure values for all mass flow rates compared to the numerical calculations. This discrepancy is observed across all tested fluids and suggests that while both methods follow a similar trend, the simulations tend to overestimate the total pressure. This graphical comparison highlights that numerical calculations provide a good baseline, but simulations may offer a more comprehensive understanding of pressure behavior under different conditions. Further investigation is needed to identify the factors contributing to the observed differences and refine both methods' accuracy.

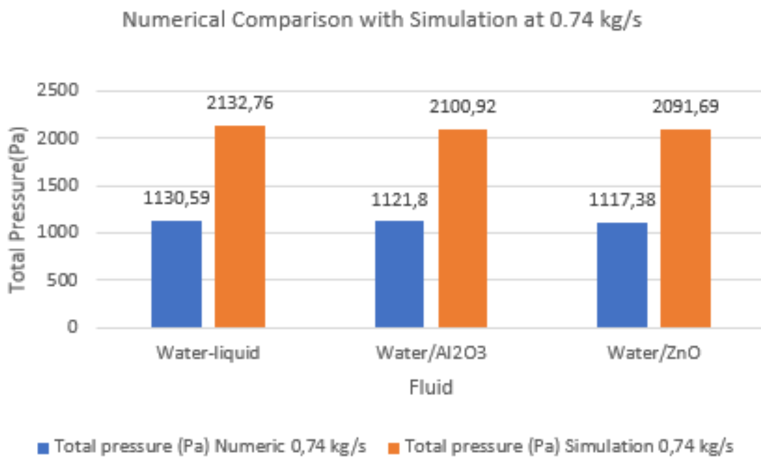

(a)

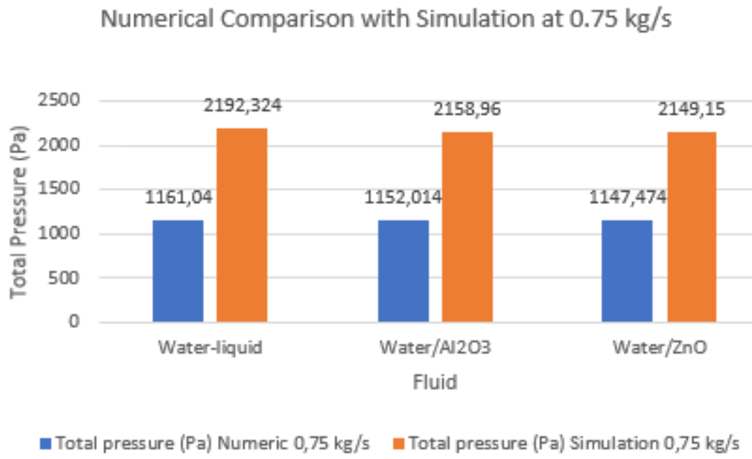

(b)

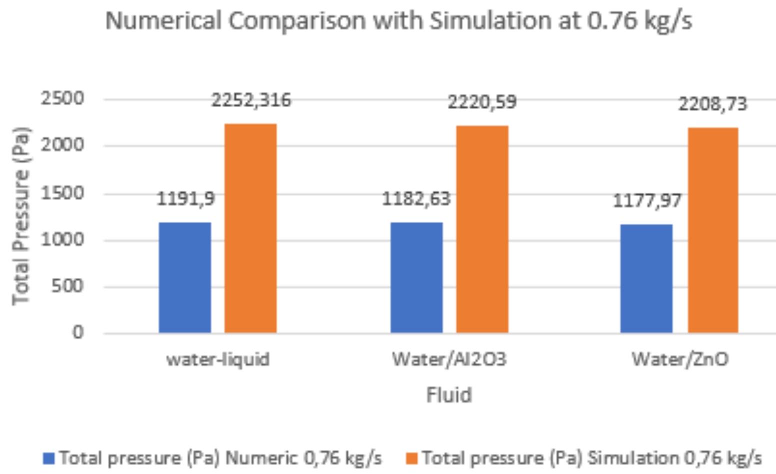

(c)

Fig. 10. Differences between numerical results and simulation results result for (a) 0.74 kg/s, (b) 0.75 kg/s, (c) 0.76 kg/s

4.3.1 Analysis Anova

Based on the ANOVA Table 2 results, the analysis indicates that fluid type and mass flow rate inlet significantly affect total pressure, with a significant interaction between these factors. Here is a detailed explanation of each component:

i. Effect of the Column Factor (Mass Flow Rate): The column in the ANOVA table represents the influence of mass flow rate, showing a p-value of 0 and an F-value of 29.5. This indicates that changes in mass flow rate significantly affect total pressure. With a p-value < 0.05, we can conclude that variations in mass flow rate lead to substantial changes in measured pressure, likely due to changes in flow dynamics that impact the distribution of pressure within the system.
ii. Effect of the Row Factor (Fluid Type): The row in the ANOVA table represents the effect of the fluid type used, with a p-value of 0 and a very high F-value of 13271.67. This indicates that fluid type significantly and strongly influences the measured pressure. With a p-value < 0.05, the statistical differences between fluid types are confirmed to produce

substantial variations in pressure, likely due to differences in physical properties such as viscosity or density of each fluid; this is similar to a previous study [32].

iii. Interaction between Fluid Type and Mass Flow Rate: The interaction between the column and row factors has a p-value of 0.0355 and an F-value of 4.47, indicating a significant interaction between fluid type and mass flow rate in affecting pressure. This means that the effect of mass flow rate on pressure is inconsistent across all fluid types; changes in mass flow rate can affect pressure differently depending on the fluid type used. This interaction shows that specific combinations of fluid type and mass flow rate result in pressure effects that the independent effects of each factor cannot fully explain; this theory is taken from the previous study [19,29,33,34].

Table 2
Anova Results

Source	SS	df	MS	F	Prob>F
Columns	2064.4	2	10324.2	29.5	0
Rows	4645367.4	1	4645367.4	13271.67	0
Interaction	3125.8	2	1562.9	4.47	0.0355
Error	4200.3	12	350		
Total	4673341.8	17			

Overall, these ANOVA results demonstrate that fluid type and mass flow rate inlet have significant independent effects on pressure, and there is also an interaction between the two. This finding highlights the importance of considering the combined influence of fluid type and mass flow rate in applications involving pressure measurement or control, as each combination can yield different outcomes in the system. These are taken similarly to the previous study [35–37].

4.3.2 Discussion of Result Analysis

Overall, the results of this study indicate that variations in fluid types and mass flow rates significantly impact pressure distribution in a rough-walled U-pipe. Fluids containing nanoparticles (Water/Al_2O_3 and Water/ZnO) exhibit lower pressure compared to pure water, which can be attributed to an increase in effective viscosity and more significant energy dissipation within the mixed fluids. These findings align with existing literature, where previous studies also reported similar effects of nanoparticles on fluid flow and pressure distribution [3,17].

Practically, these results have important implications for engineering applications, particularly in the design and optimization of industrial piping systems and heat exchangers. Understanding how fluid type and mass flow rate affect total pressure can help engineers optimize design parameters to achieve higher flow efficiency, reduce energy consumption, and ensure system reliability. By employing advanced turbulence models such as RANS and LES, prediction accuracy in CFD simulations can be improved, enabling more profound analysis and more precise design solutions [21].

4.3.3 Total effect of lowest and highest pressure on energy

The variation in total pressure within a system, particularly between the lowest pressure produced by Water/ZnO at 2091.69 Pa and the highest at 2252.316 Pa, can be critically examined through potential energy and fluid dynamics. Lower pressure is typically indicative of reduced potential energy within the system, suggesting a corresponding decrease in the kinetic energy of the fluid molecules [38]. This relationship constrains the system's ability to perform work or facilitate movement, limiting dynamic processes such as fluid flow and energy transfer. In contrast, elevated pressure increases kinetic energy among the liquid molecules, translating into higher potential energy that enables the system to execute more work. Furthermore, higher pressure conditions can enhance reaction rates in chemical processes, thereby accelerating reactions that demand additional energy input [39].

The concept of potential energy can be effectively illustrated through a basketball analogy. A fully inflated basketball, representing high pressure, possesses more incredible potential energy, allowing it to rebound higher when dropped; this theory is taken at [40]. Conversely, an under-inflated basketball, or at low pressure, will not bounce as high due to its diminished potential energy. This analogy highlights that higher pressure generates more incredible energy to facilitate movement or other changes within the system. Therefore, the differences in total pressure produced by Water/ZnO hold considerable implications for the potential energy dynamics at play, where lower pressure signifies diminished energy while higher pressure corresponds to increased potential energy that enhances fluid dynamics efficiency; this theory is taken at [40]. A comprehensive understanding of these relationships is essential for the design and optimization of systems that depend on precise control of pressure and energy across a range of technological applications [41].

5. The Applications Relevant in The Future and Suggestions for Future Researchers

5.1 The Application Relevant in The Future

Several things from this study can be applied in the future; the following is an example:

i. Industrial Pipe Systems: Optimizing the design and operation of U-bend pipes for transporting various fluids, ensuring better flow efficiency and pressure control in industrial installations.
ii. Heating and Cooling Systems: Using nanofluids with U-bend pipes in heating and cooling systems enhances heat transfer efficiency and maintains stable operational temperatures.
iii. Water and Waste Treatment: Applying nanofluids to improve the efficiency of water and waste treatment systems that use U-bend pipes, benefiting from modified flow characteristics to reduce buildup and blockages.
iv. Microfluidic Power Systems: Developing microfluidic devices using U-bend pipes and nanofluids for applications such as micropower generation and precise flow sensors.

5.2 Suggestions for Future Researchers

After conducting this research, there are several suggestions from the researcher for future researchers, the following are the suggestions:

i. Expand the Range of Fluids Tested: Investigate additional fluids or fluid mixtures to compare their pressure and flow characteristics in U-bend pipes, potentially identifying fluids with better performance.
ii. Long-Term Studies: Conduct long-term tests to observe the stability and durability of fluid properties over extended periods and under various environmental conditions using U-bend pipes.
iii. Particle Size and Concentration Variations: Explore the effects of varying nanoparticle sizes and fluid concentrations to refine pressure and flow performance in U-bend pipes.

iv. Simulation Accuracy: Improve simulation models to reduce error rates, especially at higher mass flow rates, and validate these models with experimental data in U-bend pipes.
v. Interdisciplinary Approach: Collaborate with materials science and mechanical engineering researchers to develop new fluid formulations with properties tailored for specific applications in U-bend pipes.
vi. Consider Additional Nanofluids: Future research could explore a wider variety of nanofluids, including those with different particle sizes, shapes, and concentrations, to assess their effects on pressure dynamics in U-bend pipelines; reference is taken from the previous study [35].

6. Conclusions

This study provides valuable insights into how different fluids behave under varying mass flow rates in U-bend pipes:

i. Water-Liquid: Shows the highest-pressure values, likely due to its density and increased wall friction.
ii. Water/Al_2O_3 Mixture: Exhibits slightly lower pressures than water-liquid, attributed to the increased viscosity and thermal conductivity from the nanoparticles.
iii. Water/ZnO Mixture: The lowest pressure values suggest less flow resistance, which could be advantageous in systems requiring lower pressure loads.

The ANOVA analysis confirms that fluid type and mass flow rate significantly affect pressure, with an interaction effect between the two. This highlights the importance of considering both factors in pressure control applications using U-bend pipes, driving potential innovations in various practical scenarios. Exploring these recommendations and applications could further enhance the understanding and utility of fluid dynamics in practical scenarios using U-bend pipes.

Acknowledgment
This research is the output of the Fluid Mechanics and Heat Transfer course in the Energy Plant Engineering Technology Study Program at the State University of Malang.

References
[1] Aldlemy, Mohammed, Sumaiya Jarin Ahammed, Edgar Darío Obando, and Maryam Bayatvarkeshi. "Numerical simulation on the effect of pipe roughness in turbulent flow." *Knowledge-Based Engineering and Sciences* 3, no. 1 (2022): 37-44.
[2] Gnambode, P. S., P. Orlandi, Meryem Ould-Rouiss, and Xavier Nicolas. "Large-eddy simulation of turbulent pipe flow of power-law fluids." *International Journal of Heat and Fluid Flow* 54 (2015): 196-210. https://doi.org/10.1016/j.ijheatfluidflow.2015.05.004
[3] Moukalled, Fadl, Luca Mangani, Marwan Darwish, F. Moukalled, L. Mangani, and M. Darwish. *The finite volume method*. Springer International Publishing, 2016. https://doi.org/10.1007/978-3-319-16874-6
[4] Apalowo, Rilwan. "Numerical study of different models for turbulent flow in 90 pipe bend." *U. Porto Journal of Engineering* 8, no. 2 (2022): 121-134. https://doi.org/10.24840/2183-6493_008.002_0010
[5] Arifin, Zainal, Muhammad Fuadi Hakimi, Syamsul Hadi, Singgih Dwi Prasetyo, and Watuhumalang Bhre Bangun. "The Impact of CuO Nanofluid Volume Fraction on Photovoltaic-Thermal Collector (PV/T) Performance." (2024): 2342-2350. https://doi.org/10.5109/7236877
[6] Prasetyo, Singgih Dwi, Zainal Arifin, Aditya Rio Prabowo, and Eko Prasetya Budiana. "Investigation of the addition of fins in the collector of water/Al2O3-based PV/T system: Validation of 3D CFD with experimental study." *Case Studies in Thermal Engineering* 60 (2024): 104682. https://doi.org/10.1016/j.csite.2024.104682

[7] Ferziger, Joel H., Milovan Perić, and Robert L. Street. *Computational methods for fluid dynamics*. springer, 2019. https://doi.org/10.1007/978-3-319-99693-6
[8] Nakayama, Yasuki. "Computational Fluid Dynamics", *Introduction to Fluid Mechanics* (2018):293-327. https://doi.org/10.1016/B978-0-08-102437-9.00015-2
[9] Kund, Nirmal Kumar. "Numerical modeling for thermal management of fuel cell by using Al2O3, SiC and CuO water based nanofluids." *International journal of scientific research in computer science, engineering and information technology (IJSRCSEIT)* 2, no. 5 (2017): 888-894.
[10] Mehra, Diya, Priyanka Sond, and Reena Agnihotri. "A Novel Approach to Solve Numerical Methods Using Matlab Programming."
[11] Mauludin, Mochamad S., Agung Nugroho, Arief Hidayat, and Singgih D. Prasetyo. "Simulation of AI-Based PID Controllers on DC Machines Using the MATLAB Application." *Journal Européen des Systèmes Automatisés* 57, no. 1 (2024). https://doi.org/10.18280/jesa.570127
[12] Indurain, B., David Uystepruyst, François Beaubert, Sylvain Lalot, and Á. Helgadóttir. "Numerical investigation of several twisted tubes with non-conventional tube cross sections on heat transfer and pressure drop." *Journal of Thermal Analysis and Calorimetry* 140 (2020): 1555-1568. https://doi.org/10.1007/s10973-019-08965-4
[13] De Maio, Mariangela, Beatrice Latini, Francesco Nasuti, and Sergio Pirozzoli. "Direct numerical simulation of turbulent flow in pipes with realistic large roughness at the wall." *Journal of Fluid Mechanics* 974 (2023): A40. https://doi.org/10.1017/jfm.2023.728
[14] Gersten, Klaus. "Hermann schlichting and the boundary-layer theory." In *Hermann Schlichting–100 Years: Scientific Colloquium Celebrating the Anniversary of His Birthday, Braunschweig, Germany 2007*, pp. 3-17. Berlin, Heidelberg: Springer Berlin Heidelberg, 2009. https://doi.org/10.1007/978-3-540-95998-4_2
[15] Di Bartolo, Baldassare. *Classical theory of electromagnetism*. World Scientific, 2018. https://doi.org/10.1142/10660
[16] "Flow through a Tube with U-Bend : Smooth vs Rough Walls Velocity in the Tube." (2019).
[17] Shabani, Saman, Amir Abass Abedini, and Ali Mohammadtabar. "The effect of the pipe bending angle on the pressure losses vane elbow pipes." *The Asian Review of Civil Engineering* 8, no. 1 (2019): 1-8. https://doi.org/10.51983/tarce-2019.8.1.2287
[18] Julian, James, Riki Hendra Purba, Khalees Sedeq, Fitri Wahyuni, and Thomas Junaedi. "Study of Fluid Flow Characteristics In A 90° Pipe Bend With Varying Guide Vane Length." *Journal of Applied Sciences and Advanced Technology* 6, no. 3 (2024): 99-108.
[19] Li, Haoyu, M. J. B. M. Pourquié, G. Ooms, and R. A. W. M. Henkes. "Simulation of a turbulent annulus with interfacial waves in core-annular pipe flow." *International Journal of Multiphase Flow* 154 (2022): 104152. https://doi.org/10.1016/j.ijmultiphaseflow.2022.104152
[20] Dutta, Prasun, Sumit Kumar Saha, and Nityananda Nandi. "Computational study of turbulent flow in pipe bends." *International Journal of Applied Engineering Research* 10, no. 11 (2015): 2015.
[21] Yang, Qi, Jie Dong, Tongju Xing, Yi Zhang, Yong Guan, Xiaoli Liu, Ye Tian, and Peng Yu. "RANS-Based Modelling of Turbulent Flow in Submarine Pipe Bends: Effect of Computational Mesh and Turbulence Modelling." *Journal of Marine Science and Engineering* 11, no. 2 (2023): 336. https://doi.org/10.3390/jmse11020336
[22] Benson, Michael J., Andrew J. Banko, Christopher J. Elkins, Don-Gwan An, Simon Song, Martin Bruschewski, Sven Grundmann, Daniel D. Borup, and John K. Eaton. "The 2019 MRV challenge: turbulent flow through a U-bend." *Experiments in Fluids* 61 (2020): 1-17. https://doi.org/10.1007/s00348-020-02986-8
[23] Ekat, Ann-Kathrin, Andreas Weissenbrunner, Martin Straka, Thomas Eichler, and Kilian Oberleithner. "Hybrid LES/RANS Simulations of a 90° Pipe Bend Using Different CFD Solvers." *OpenFOAM® Journal* 3 (2023): 49-65. https://doi.org/10.51560/ofj.v3.36
[24] Tijsseling, A. S. "Fluid-structure interaction in liquid-filled pipe systems: a review." *Journal of Fluids and Structures* 10, no. 2 (1996): 109-146. https://doi.org/10.1006/jfls.1996.0009
[25] Kalliadasis, S., C. Ruyer-Quil, B. Scheid, M. G. Velarde, S. Kalliadasis, C. Ruyer-Quil, B. Scheid, and M. G. Velarde. "Boundary Layer Approximation." *Falling Liquid Films* (2012): 65-93. https://doi.org/10.1007/978-1-84882-367-9_4
[26] Praks, Pavel, and Dejan Brkić. "Rational Approximation for solving an implicitly given Colebrook flow friction equation." *Mathematics* 8, no. 1 (2019): 26. https://doi.org/10.3390/math8010026
[27] Praks, Pavel, and Dejan Brkic. "Review of new flow friction equations: Constructing Colebrook explicit correlations accurately." *arXiv preprint arXiv:2005.07021* (2020). https://doi.org/10.20944/preprints202005.0243.v1
[28] Surakasi, Raviteja, Vv Prasanna Kumar, "CFD analysis of heat transfer and pressure drop characteristics of a finned tube heat." Bulletin Monumental 22, no 7 (2021):118-126.
[29] Evran, Savaş, and Mustafa Kurt. "CFD and statistical analysis of flow mass ratios on temperature and pressure drops of double pipe heat exchanger." *International Journal of Low-Carbon Technologies* 18 (2023): 771-780. https://doi.org/10.1093/ijlct/ctad056

[30] Ahmadloo, Ebrahim, Najmeh Sobhanifar, and Fatemeh Sadat Hosseini. "Computational fluid dynamics study on water flow in a hollow helical pipe." *Open Journal of Fluid Dynamics* 2014 (2014). https://doi.org/10.4236/ojfd.2014.42012

[31] Akhavan-Behabadi, M. A., Mohamad Shahidi, M. R. Aligoodarz, and Mohammad Ghazvini. "Experimental investigation on thermo-physical properties and overall performance of MWCNT–water nanofluid flow inside horizontal coiled wire inserted tubes." *Heat and Mass Transfer* 53 (2017): 291-304. https://doi.org/10.1007/s00231-016-1814-5

[32] Cerpa, Nestor G., Ikuko Wada, and Cian R. Wilson. "Effects of fluid influx, fluid viscosity, and fluid density on fluid migration in the mantle wedge and their implications for hydrous melting." *Geosphere* 15, no. 1 (2019): 1-23. https://doi.org/10.1130/GES01660.1

[33] Delgado Ruiz, Leonardo, Carlos Humberto Acevedo Peñaloza, and Guillermo Valencia Ochoa. "Effect of the mass flow rate on the heat transfer phenomena in a shell and tube heat exchanger." *International Journal of Applied Engineering Research* 13, no. 14 (2018) (2018): 11387-11391.

[34] Launder, Brian Edward, and Bahrat I. Sharma. "Application of the energy-dissipation model of turbulence to the calculation of flow near a spinning disc." *Letters in heat and mass transfer* 1, no. 2 (1974): 131-137. https://doi.org/10.1016/0094-4548(74)90150-7

[35] Akaje, Wasiu, and B. I. Olajuwon. "Impacts of Nonlinear thermal radiation on a stagnation point of an aligned MHD Casson nanofluid flow with Thompson and Troian slip boundary condition." *Journal of Advanced Research in Experimental Fluid Mechanics and Heat Transfer* 6, no. 1 (2021): 1-15.

[36] Morita, J., H. Mamori, and T. Miyazaki. "Direct numerical simulation of the backward-facing step turbulent flow controlled by traveling wave-like body force." *International Journal of Heat and Fluid Flow* 95 (2022): 108964. https://doi.org/10.1016/j.ijheatfluidflow.2022.108964

[37] Jehad, D. G., G. A. Hashim, A. Kadhim Zarzoor, and CS Nor Azwadi. "Numerical study of turbulent flow over backward-facing step with different turbulence models." *Journal of Advanced Research Design* 4, no. 1 (2015): 20-27.

[38] Arifin, Zainal, Nuha Khairunisa, Budi Kristiawan, Singgih Dwi Prasetyo, and Watuhumalang Bhre Bangun. "Performance analysis of nanofluid-based photovoltaic thermal collector with different convection cooling flow." *Civil Engineering Journal* 9, no. 8 (2023): 1922-35. https://doi.org/10.28991/CEJ-2023-09-08-08

[39] Streeter, Victor, L., Benam Wylie, E., "Fluid mechanics (seventh ed)." (1979).

[40] Munson, Bruce R., Theodore H. Okiishi, Wade W. Huebsch, and A. P. Rothmayer. *Fluid Mechanics, SI Version*. Wiley, 2013.

[41] Cengel, Yunus A. "Thermodynamics: an engineering approach." (2011).